Journal of Power Sources 196 (2011) 977–987

Contents lists available at ScienceDirect

Journal of Power Sources

journal homepage: www.elsevier.com/locate/jpowsour

Effects of bi-layer $La_{0.6}Sr_{0.4}Co_{0.2}Fe_{0.8}O_{3-\delta}$-based cathodes on characteristics of intermediate temperature solid oxide fuel cells

Sea-Fue Wang[a,*], Yuh-Ruey Wang[a], Chun-Ting Yeh[a], Yung-Fu Hsu[a], San-Der Chyou[b], Win-Tai Lee[b]

[a] Department of Materials and Mineral Resources Engineering, National Taipei University of Technology, Taipei city 106, Taiwan, ROC
[b] Taiwan Power Research Institute of Taiwan Power Company, Shulin City, Taipei County, Taiwan, ROC

ARTICLE INFO

Article history:
Received 18 July 2010
Received in revised form 24 August 2010
Accepted 25 August 2010

Keywords:
Solid oxide fuel cell
Bi-layer cathode
Polarization
Cell performance

ABSTRACT

In this study, anode-supported planar IT-SOFCs, with a thin $Sm_{0.2}Ce_{0.8}O_{2-\delta}$ (SDC) electrolyte film and a bi-layer cathode, are fabricated using tape-casting and screen-printing processes. The bi-layer cathode consists of a current collector $La_{0.6}Sr_{0.4}Co_{0.2}Fe_{0.8}O_{3-\delta}$ (LSCF) layer and a functional LSCF–SDC composite layer in various thicknesses. Microstructure studies reveal that the interfaces among various layers show good adhesion, except for Cell A equipped with a cathode of pure LSCF. Cell A reports the lowest ohmic (R_0) and polarization (R_P) resistances. R_P, which increases with the thickness of the LSCF–SDC composite layer in the cathode, rises rapidly as the temperature drops, particularly at temperatures $\leq$550 °C. This indicates the high electrical conductivity of the cathode as a major contribution to the decrease of R_P at 500 °C. The best cell performances are observed at 650 °C for all cases, in which Cell A shows a maximum power density of 1.51 W cm^{-2} and an open circuit voltage of 0.80 V. Considering both of the electrical and the mechanical integrity of the single cell, insertion of the composite layer is required to guarantee a good adhesion of cathode layer to electrolyte layer. However, the thickness of the composite layer should be retained as thin as possible to minimize the R_0 and R_P and maximize the cell performance.

1. Introduction

Solid oxide fuel cell (SOFC) system is considered to have superior potential for commercialization thanks to its high energy conversion efficiency, self-reforming ability, compatibility with common hydrocarbon fuels, use of solid state materials, and no need of noble metals as catalysts [1]. SOFC can be used in large-size stationary power facilities or applied to heat and power generation for homes and businesses as well as auxiliary power units for electrical systems in transportation vehicles. Planar-type SOFCs are superior to those with tubular designs because of their simple manufacturing process and the promise of a high power density [2].

In recent years, enormous research efforts have been invested on the development of intermediate temperature SOFCs (IT-SOFCs) capable of operating at temperatures between 500 and 700 °C [3]. However, the performance of IT-SOFCs depends strongly on the ionic conductivity of electrolyte and the polarization resistance (R_P) of the electrodes [4]. The former problem can be solved by using alternative electrolytes with higher ionic conductivity at low temperatures, such as $La_{0.9}Sr_{0.1}Ga_{0.8}Mg_{0.2}O_{3-\delta}$ (LSGM) and $Sm_{0.2}Ce_{0.8}O_{2-\delta}$ (SDC) or by using a thin yttria-stabilized zirconia (YSZ) electrolyte film [5]. Since oxygen reduction reaction is generally thought to be more difficult to activate on SOFCs operating at intermediate temperatures, the cathode is often the limiting resistance of the SOFC cell because of its large overpotential [6].

While $La_{1-x}Sr_xMnO_3$ (LSM) remains the preferred cathode material for use with YSZ at high temperatures (>850 °C), alternative cathodes are required for YSZ to operate at lower temperatures as its performance tends to be poorer below 800 °C [6,7]. The performance of LSM cathode declines drastically as the operating temperature drops, due to its low oxygen ion conductivity and high activation energy for oxygen dissociation [6,8]. Accordingly, several approaches have been developed to improve the performance of the cathodes, including: (a) using mixed ionic/electronic conductors (MIECs) like $La_{0.6}Sr_{0.4}Co_{0.2}Fe_{0.8}O_{3-\delta}$ (LSCF) [9], $Ba_{0.5}Sr_{0.5}Co_{0.8}Fe_{0.2}O_{3-\delta}$ (BSCF) [10], $La_{0.75}Sr_{0.25}CuO_{2.5-\delta}$ [11] and $Pr_{0.35}Nd_{0.35}Sr_{0.3}MnO_{3-\delta}$ (PNSM) [12]; (b) optimizing the cathodic microstructure by adjusting the porosity and grain size of the materials [13]; (c) employing composite cathodes, such as mixtures of two cathode materials (e.g. $SrSc_{0.2}Co_{0.8}O_{3-\delta}$ + $Sm_{0.5}Sr_{0.5}CoO_{3-\delta}$) [14], cathode/electrolyte materials (e.g. LSCF–$Gd_{0.1}Ce_{0.9}O_{1.95}$, GDC) [15], or cathode materials with additions of Ag, Pd, or Pt in the form of nano-sized particles [16–18]; (d) exploiting functionally graded cathodes [19], and (e) applying bi-layer or multilayer composite cathodes [4,20,21].

* Corresponding author. Present address: Department of Materials and Mineral Resources Engineering, National Taipei University of Technology, 1, Sec. 3, Chung-Hsiao E. Rd., Taipei 106, Taiwan, ROC. Tel.: +886 2 2771 2171x2735; fax: +886 2 2731 7185.
E-mail addresses: sfwang@ntut.edu.tw, seafuewang@yahoo.com (S.-F. Wang).

0378-7753/$ – see front matter © 2010 Elsevier B.V. All rights reserved.
doi:10.1016/j.jpowsour.2010.08.064

Adding electrolyte to cathode and forming a cathode–electrolyte composite cathode has been found to result in dramatic improvement of the electrochemical performance of the cathode [8]. This phenomenon is attributed to the extension of the three-phase boundary (TPB) of the electrolyte (ionic conductor), cathode (electronic conductor) and gas phase (oxygen or air used as an oxidant). Additional benefits include better adhesion and thermal expansion match to the electrolyte layer [22]. Composite electrodes commonly containing 40–60 wt% of electrolyte are characterized by low electrical conductivity, a disadvantage that can be resolved by using a design of bi-layer electrodes. The functional layer, which directly contacts the electrolyte, needs to have good thermal and chemical compatibility with the electrolyte and provide high electrochemical activity for oxygen reduction. The outer current collector layer, on the other hand, is usually composed of high-conductivity materials to facilitate a uniform current distribution along the cathode and to help capture the electrons from the outer circuit to the TPB of the cathode functional layer [20]. Similar to bi-layer cathodes, multilayer cathodes and functionally graded cathodes are fabricated through inserting layers with different cathode/electrolyte ratios to guarantee a smooth transition from one cathode material to another cathode material [23] or from one electrolyte material to another electrolyte material [4,21] in the composite cathode. However, these techniques often require complicated layering processes for producing SOFC cells.

Using impedance spectroscopy, Murray et al. reported the transport processes of three types of cathode electrodes, including pure LSM electrode, LSM–YSZ composite and LSM/LSM–YSZ bi-layer electrodes [24,25]. The addition of electrolyte materials such as YSZ or SDC in LSM cathode is essential to ensure high electrochemical performance for SOFCs with YSZ electrolyte and LSM cathode. In the present study, a bi-layer cathode was fabricated for anode-supported planar IT-SOFCs with a thin SDC electrolyte film. The functional layer adjacent to the SDC electrolyte film is a screen printed LSCF–SDC composite layer while the second (outer) current collector layer is a screen printed pure LSCF film. Compared to other cathode materials, LSCF, a mixed ionic and electronic conductor, reports a greater electrical conductivity and higher surface oxygen exchange coefficients and oxide-ion diffusivities [7,8]. In addition to its role of providing active sites for oxygen reduction reaction, LSCF was selected as a current collector layer in this study. SOFCs with various thicknesses of the functional LSCF–SDC composite layer and current collector LSCF layer were built and characterized through microstructural and electrochemical performance studies. The effects of the relative thickness on the electrochemical performance of the SOFCs were investigated and discussed.

2. Experimental procedure

2.1. Raw materials

Commercially available raw materials for SOFC, including $Sm_{0.2}Ce_{0.8}O_{2-\delta}$ (SDC; Fuel Cell Materials, USA; d_{50} = 0.53 μm and BET surface area = 6.2 $m^2\,g^{-1}$), $La_{0.6}Sr_{0.4}Co_{0.2}Fe_{0.8}O_{3-\delta}$ (LSCF: Fuel Cell Materials, USA; d_{50} = 0.99 μm and BET surface area = 5.4 $m^2\,g^{-1}$), and NiO (anode functional layer: Fuel Cell Materials, USA; current collector layer: SHOWA, Japan), were used in this study. Two kinds of NiO powders were used to build the SOFCs. One with a smaller particle size (d_{50} = 0.8 μm and BET surface area = 3.4 $m^2\,g^{-1}$) was used for anode functional layers to increase the TPB and, by extension, the electrochemical activity; the other with a larger particle size (d_{50} = 10.1 μm and BET surface area = 0.06 $m^2\,g^{-1}$) was used for the anode current collector layer to minimize the sintering shrinkage mismatch with other layers and to control the layer porosity.

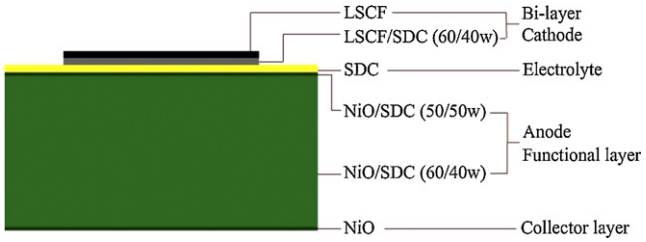

Fig. 1. Schematically drawn of the anode-supported single cell structure of IT-SOFC with bi-layer cathode.

2.2. Fabrication of single cells

Fig. 1 illustrates the schematically drawn cell structure of the anode-supported IT-SOFC with the bi-layer cathode. The anode-supported substrates incorporate a SDC electrolyte layer and a three-layer anode composed of a current collector layer (outer layer) of pure NiO and two functional layers of NiO–SDC composites with ratios of 60 wt%/40 wt% and 50 wt%/50 wt%, respectively. The thin 50 wt% NiO/50 wt% SDC composite layer provides a good contact with the adjacent electrolyte layer. Ceramic raw powders were mixed with 19.7 wt% of organic binder (B74001; Ferro), 25.6 wt% of solvent (60 wt% toluene/40 wt% ethanol) and 0.7 wt% of dispersant (M1201; Ferro) to form colloidal ceramic suspensions. The anode-supported substrates were then built via tape-casting process, and the dried and laminated tapes drilled into discs. The discs with a size of 25 mm in diameter and 0.5 mm in thickness were then co-fired at 1400 °C for 2 h at a heating rate of 2 °C min^{-1}.

The bi-layer cathode was prepared by screen-printing a functional layer and a current collector layer on the anode-supported SDC substrate in sequence. Cathode powders were mixed with a proper amount of terpineol (solvent) and ethyl cellulose (binder) to form a paste. The first layer was a LSCF–SDC composite (60 wt%/40 wt%) and the outer layer a pure LSCF. The cathode was then fired at 1000 °C for 2 h. Table 1 shows the designs of single cells composed of a cathode functional layer and a current collector layer in various thicknesses as prepared in this study.

2.3. Microstructural and electrochemical characterizations

Scanning electron microscopy (SEM, Hitachi S4700) studies on the fracture surfaces of the sintered cells were conducted to examine the cross-sectional microstructures. The porosity of the cathode

Table 1
Design of the anode-supported single SOFC cells with a cathode functional layer and a current collector layer in various thicknesses.

Structure	Material	Cell A	Cell B	Cell C	Cell D	Cell E
Cathode current collector layer	LSCF	40 μm	30 μm	20 μm	10 μm	0 μm
Cathode functional layer	LSCF/SDC (60 wt%/40 wt%)	0 μm	10 μm	20 μm	30 μm	40 μm
Electrolyte layer	SDC	13 μm	13 μm	13 μm	13 μm	13 μm
Anode functional layer	NiO/SDC (50 wt%/50 wt%)	6 μm	6 μm	6 μm	6 μm	6 μm
Anode functional layer	NiO/SDC (60 wt%/40 wt%)	460 μm	460 μm	460 μm	460 μm	460 μm
Anode current collector layer	NiO	20 μm	20 μm	20 μm	20 μm	20 μm

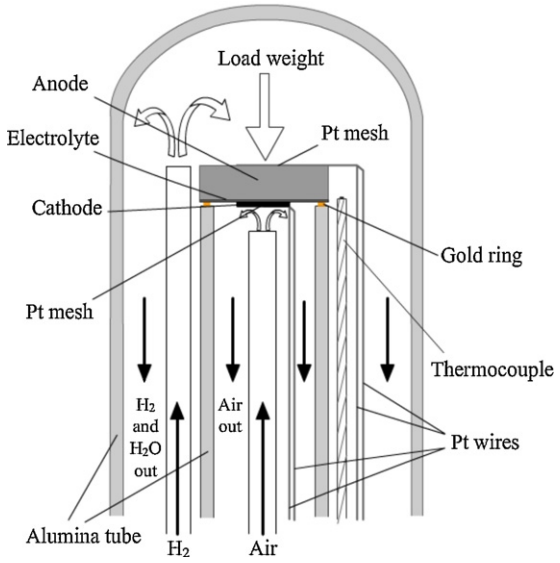

Fig. 2. Configuration of a test cell setup for high temperature electrochemistry measurement.

layer was characterized using mercury porosimetry (Micromeritics AUTOPORE 9520/NTUPT03). The electrochemical performance of the single cells was measured at the setup of a commercially available ProboStat (NorECs, Norway) shown in Fig. 2. Platinum meshes were used as current collectors both at the cathode and at the anode, and proper electrical contact was established through platinum lead wires. The cells were mounted on the end of an

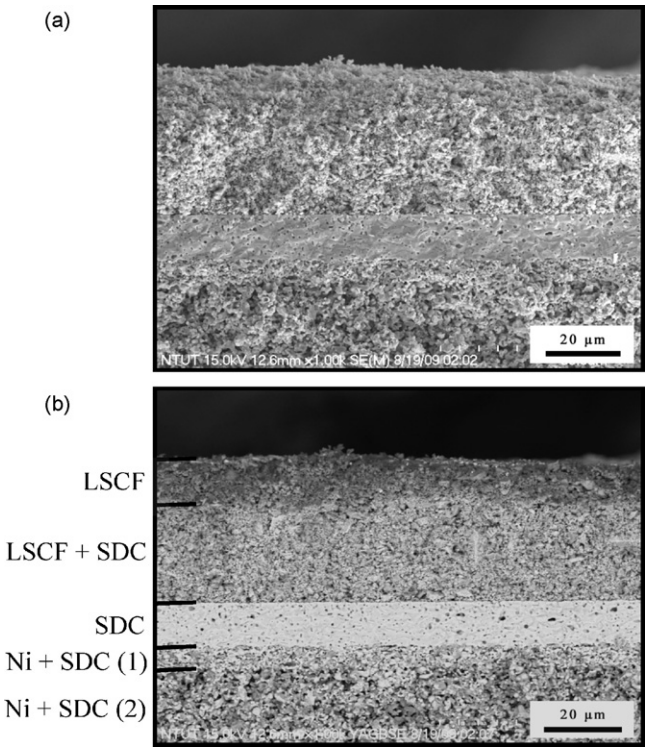

Fig. 3. (a) SEM and (b) BEI micrographs of Cell D after electrochemical measurements.

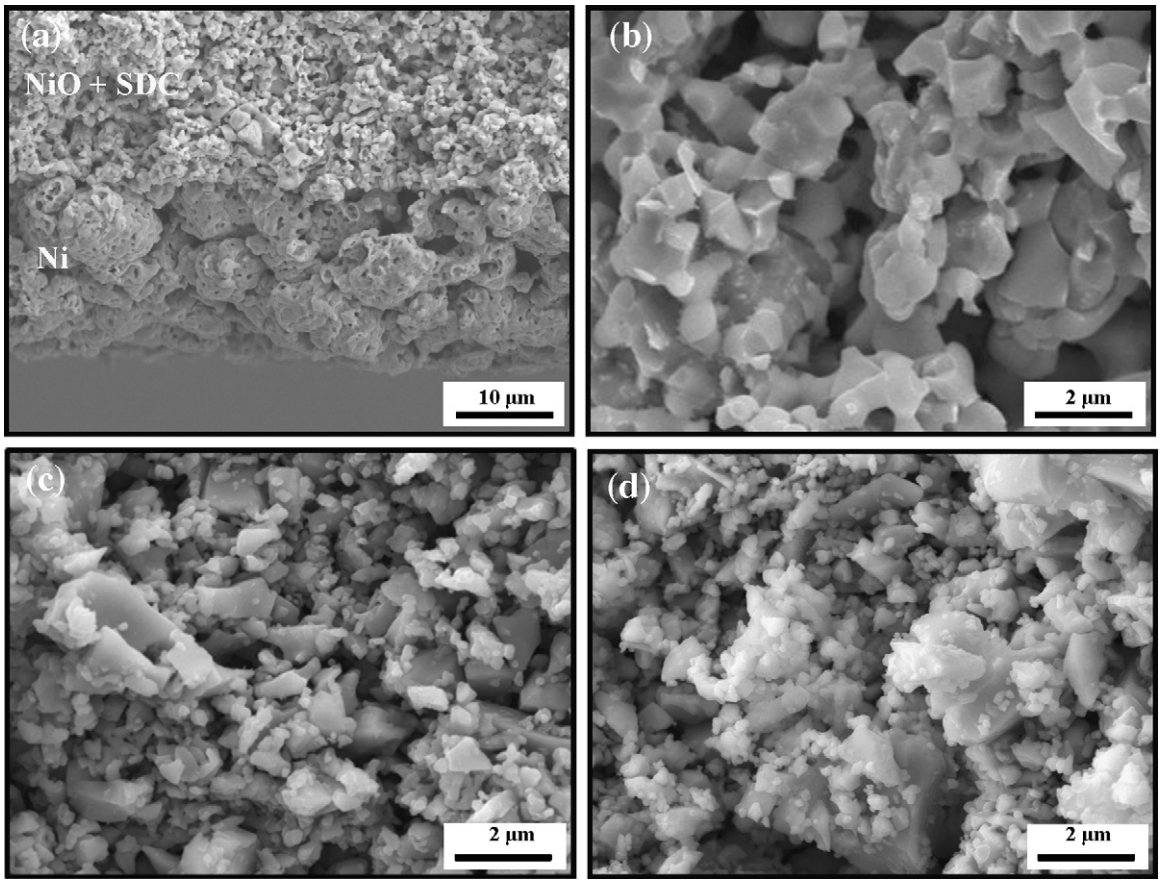

Fig. 4. SEM micrographs of the fracture cross-sectional view of (a) the interface of pure NiO and NiO–SDC composite anode, (b) NiO–SDC composite anode, (c) pure LSCF cathode layer and (d) LSCF–SDC composite cathode layer in the anode-supported single cells, after electrochemical measurements.

alumina tube, sealed with a gold ring, and kept inside a vertical split-type furnace. A constant spring loaded force was applied to the cell. The gas tightness of the cells was tested at room temperature before start-up. Then the cell was heated up to 1000 °C under a nitrogen atmosphere (20 sccm) on both sides of the cell at a heating rate of 2 °C min^{-1}, and the gold ring softened to form a gas-tight seal. The next step saw the temperature decreased to 700 °C for anode reduction under hydrogen atmosphere before electrochemical measurements. The reduction of NiO to metallic Ni for the anode of the single cells was then achieved by gradual replacement of nitrogen with hydrogen. Hydrogen bubbled through water at room temperature was supplied to the anode side as fuel gas, and compressed air was supplied to the cathode side as oxidant gas. During testing, the flow rates of hydrogen and air were kept, respectively, at 40 and 160 sccm by electronic mass flow controllers. The current density as a function of cell voltage (*I–V* curves) was evaluated under different applied loads across the cell, and measurements were carried out at 500–700 °C at intervals of 50 °C. Electrochemical impedance spectra (EIS) were measured after holding the cells under OCV for 15 min at the temperatures ranging from 500 to 700 °C. The EIS measurements were performed with a four-lead two-electrode configuration using a multi-channel potentiostat/galvanostat (Solartron 1470E) and a 1260 frequency response analyzer with a computer interface and Corr-view software. The frequency range was from 10^5 to 0.015 Hz, and the signal amplitude read 10 mV. *I–V* curves and power curves were obtained using linear sweep from OCV to 0.2 V at a sweep rate of 5 mV s^{-1}. After testing, the microstructure of the cells was examined by SEM.

3. Results and discussion

Fig. 3 shows the SEM and backscattering electron image (BEI) micrographs of the Cell D after electrochemical measurements, which represent a typical microstructure for the single cells prepared in this study. It can be observed that the SDC electrolyte with a thickness of approximately 13 μm is crack free and dense with some scattering closed pores whose porosity allows no passage for gas leakage in the SOFC electrolyte. The interfaces among the anode, electrolyte, and cathode layers for all cells showed no sign of crack, discontinuity, or delamination. Detailed SEM images of the anode, electrolyte and cathode layers in Cell D are presented in Fig. 4. The anode electrode consists of three layers with a total thickness of approximately 0.5 mm, including a current collector layer of NiO (≈20 μm) and two functional composite layers (with the NiO/SDC ratios of 60 wt%/40 wt% and 50 wt%/50 wt%, and the thicknesses of ≈460 and ≈6 μm, respectively). XRD analysis confirmed the complete reduction of NiO to Ni at the anode after the electrochemical test. Both the anode and cathode layers were marked with the presence of porous microstructures. As shown in Fig. 4(a), the Ni layer has a high level of agglomeration, a size of 10–20 μm, and a high level of interconnected porosity. The anode functional layer of Ni–SDC (Fig. 4(b)) has a grain size much coarser than that of the cathode functional layers of LSCF (Fig. 4(c)) and LSCF/SDC (Fig. 4(d)). This is because the anode was sintered at a much higher temperature as compared to the cathode (1400 °C versus 1000 °C). The porosity contents of the LSCF layer and 60 wt% LSCF–40 wt% SDC composite layer, measured by mercury porosimetry, read 45.5% and 40.4%, respectively. Therefore, the cathode has good interconnecting pores and a fine grain microstructure, leading to a high specific area of the cathode (2.76 m^2 g^{-1} and 2.53 m^2 g^{-1} for LSCF layer and 60 wt% LSCF–40 wt% SDC composite layer, respectively). Comparing as shown in Fig. 5, the XRD results on the mixture of LSCF and SDC heated at 1000 °C for 2 h confirm that there was no chemical reaction between LSCF and SDC when they were heated at 1000 °C during firing.

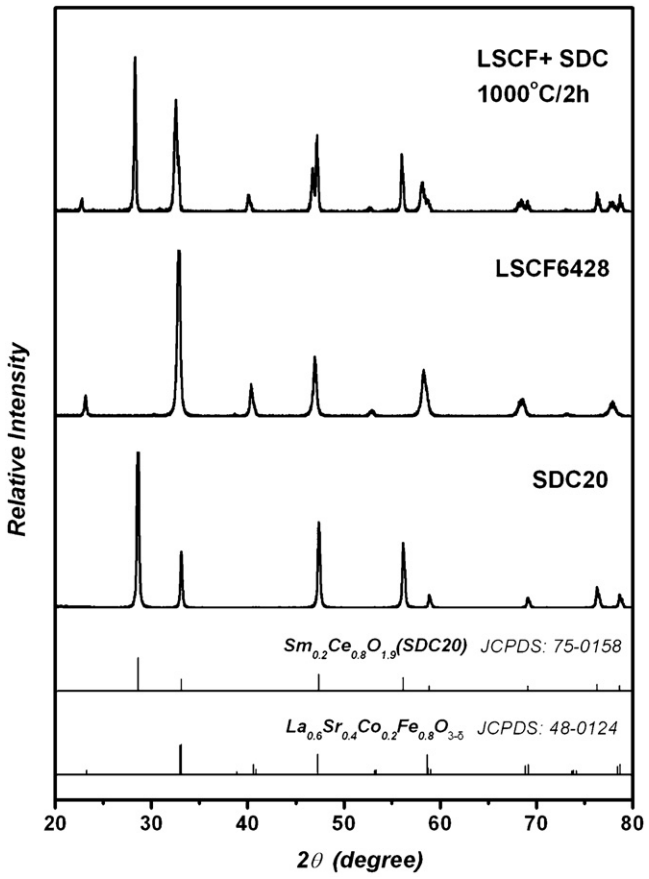

Fig. 5. XRD results of the mixture of LSCF and SDC heated at 1000 °C for 2 h.

Fig. 6 shows the Nyquist plots of electrochemical impedance spectra of the single cells containing bi-layer cathodes with a LSCF–SDC layer and a LSCF layer in various thicknesses. It can be observed that the inductive process coming from the measurement setup is appreciable at the high frequency of the spectra. As discussed in the literature [24,25], the highest frequency intercept of the impedance spectra gives the total ohmic resistance of the cell (R_0), including the resistive contributions of the electrolyte, the two electrodes, the current collectors, and the lead wires. The lowest frequency intercept gives the overall resistance of the cell, and the distance between the two intercepts corresponds to the total interfacial polarization resistance (R_P) [9]. The polarization loss from the anode side was trivial enough to be ignored as compared to its counterpart from the cathode side, a finding mirroring the observations by Huang et al., Xia et al., and Fu et al. [26–29]. Moreover, since all the anode/electrolyte assemblies of the single cells were prepared under the exactly same design and fabrication conditions in this study, the differences in R_P value observed in impedance spectra of the single cells should be solely accounted for by the differences in cathodes.

Fig. 7 and Table 2 show the temperature dependence of R_0 and R_P of the single cells containing bi-layer cathodes with a LSCF–SDC layer and a LSCF layer in various thicknesses. At the measurement temperature of 700 °C, of all the single cells, Cell A reported the lowest R_0 (0.03 Ω cm^2) and the rest of the cells were marked with the same value (0.04 Ω cm^2), both of which appeared to be lower than those reported in the literature [22,30]. Although it is generally agreed that the variation in R_0 is mainly caused by the differences in the resistance of the electrolyte, the slight differences in the R_0 of the single cells are due to the need to take into consideration of an additional contact resistance at the interface between

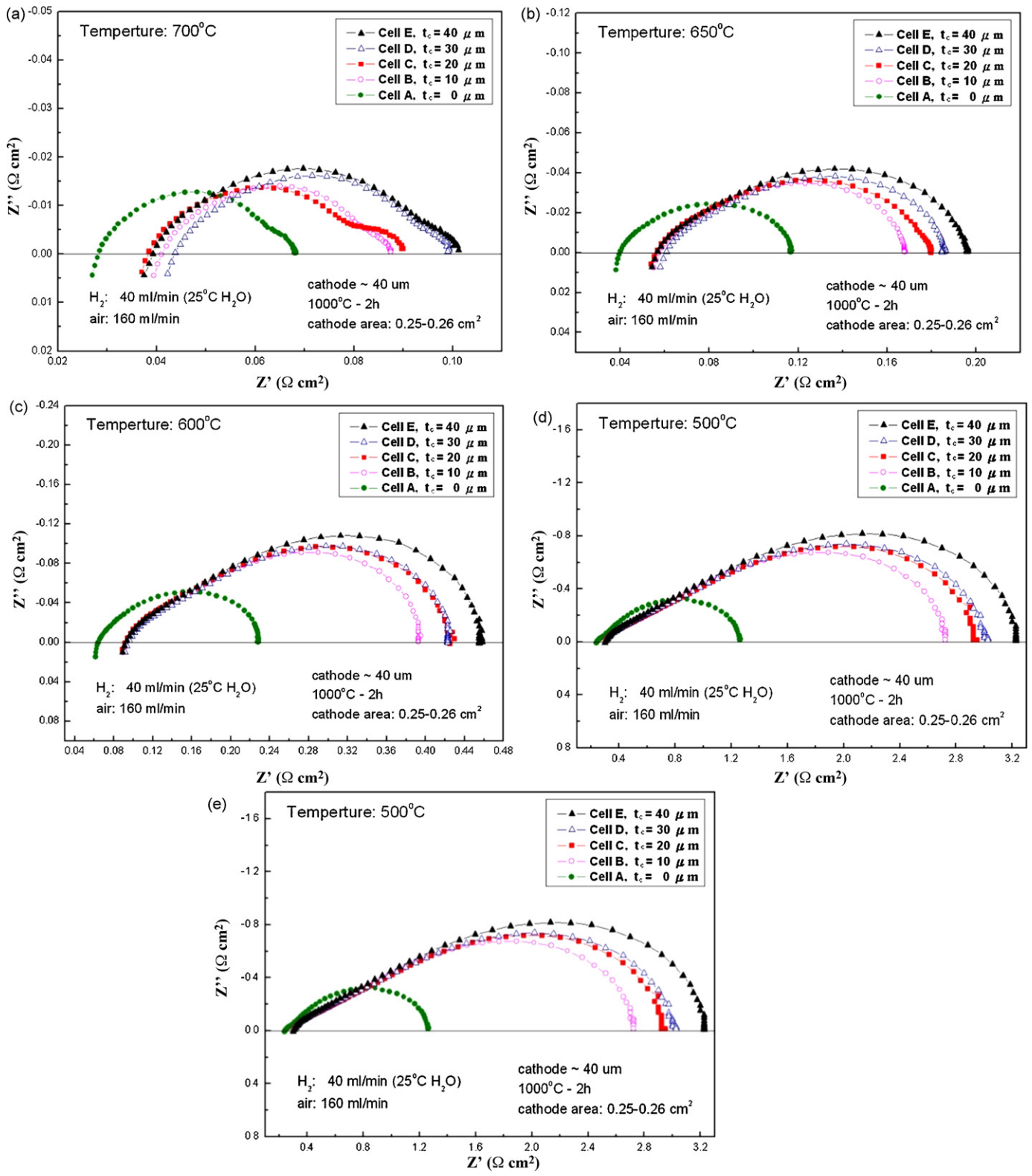

Fig. 6. Impedance spectra of the anode-supported single cells containing bi-layer cathodes composed of a LSCF–SDC layer and a LSCF layer in various thicknesses (t_c represents the thickness of the LSCF–SDC composite cathode), measured at (a) 700 °C, (b) 650 °C, (c) 600 °C, (d) 550 °C, and (e) 500 °C.

the current collector LSCF layer and the LSCF–SDC composite layer in the bi-layer cathode as well as the differences in contact resistance between the interface of LSCF cathode/SDC electrolyte and that of LSCF–SDC cathode/SDC electrolyte. Also to be noted is that the electrical conductivity of the LSCF–SDC composite is expected to be inferior as compared to that of pure LSCF. It should be noted that Cell A, with the cathode having 40 μm of pure LSCF, betrayed a poor adhesion between the LSCF cathode, since the mismatch of the thermal expansion is significant (LSCF: $16.2 \times 10^{-6}\,K^{-1}$; SDC: $12.6 \times 10^{-6}\,K^{-1}$) [22,31]. The cathode LSCF layer could be easily detached from the SDC electrolyte layer after electrochemical measurement. It can be observed that the R_0 of the single cells

Table 2
Results of R_0 and R_P electrochemical impedance spectra of anode-supported single cells measured at the temperatures ranging from 500 to 700 °C.

Sample	Impedance	700 °C	650 °C	600 °C	550 °C	500 °C
Cell A	R_0	0.025	0.036	0.061	0.121	0.227
	R_P	0.043	0.081	0.169	0.415	1.043
	$R_P/(R_0+R_P)$	0.622	0.690	0.743	0.783	0.818
Cell B	R_0	0.037	0.052	0.081	0.153	0.276
	R_P	0.050	0.117	0.315	0.851	2.485
	$R_P/(R_0+R_P)$	0.576	0.694	0.794	0.848	0.900
Cell C	R_0	0.032	0.043	0.078	0.125	0.279
	R_P	0.058	0.138	0.348	0.935	2.692
	$R_P/(R_0+R_P)$	0.644	0.763	0.816	0.882	0.906
Cell D	R_0	0.038	0.051	0.085	0.154	0.277
	R_P	0.061	0.135	0.341	0.927	2.770
	$R_P/(R_0+R_P)$	0.618	0.726	0.801	0.857	0.909
Cell E	R_0	0.033	0.048	0.082	0.152	0.275
	R_P	0.068	0.149	0.376	1.009	2.974
	$R_P/(R_0+R_P)$	0.669	0.757	0.822	0.869	0.915

R_0: ohmic resistance; R_P: polarization resistance; unit: $\Omega\,cm^2$.

increased continuously as the measurement temperature went down from 700 to 500 °C (Fig. 7(a)). This is a typical occurrence due to the dependence of the ionic conductivity of the SDC on temperature. The R_0 magnitudes of various single cells follow a similar sequence, i.e. $R_{0,Cell\ E} \approx R_{0,Cell\ D} \approx R_{0,Cell\ C} \approx R_{0,Cell\ B} > R_{0,Cell\ A}$, at all temperatures measured. The curves of R_0 for Cell A are smaller than the rest of the cells. Based on the EIS results, the presence of the composite LSCF–SDC layer was observed to trigger increase in the ohmic resistance of the single cell. At the temperature of 500 °C, the ohmic resistance increased from 0.24 $\Omega\,cm^2$ for Cell A having 40 μm of LSCF layer to 0.31 $\Omega\,cm^2$ for Cells B, Cell C, Cell D and Cell E having the LSCF–SDC composite layer, clearly identifying the low conductivity of the composite layer with SDC electrolyte addition as the major cause of the rising R_0.

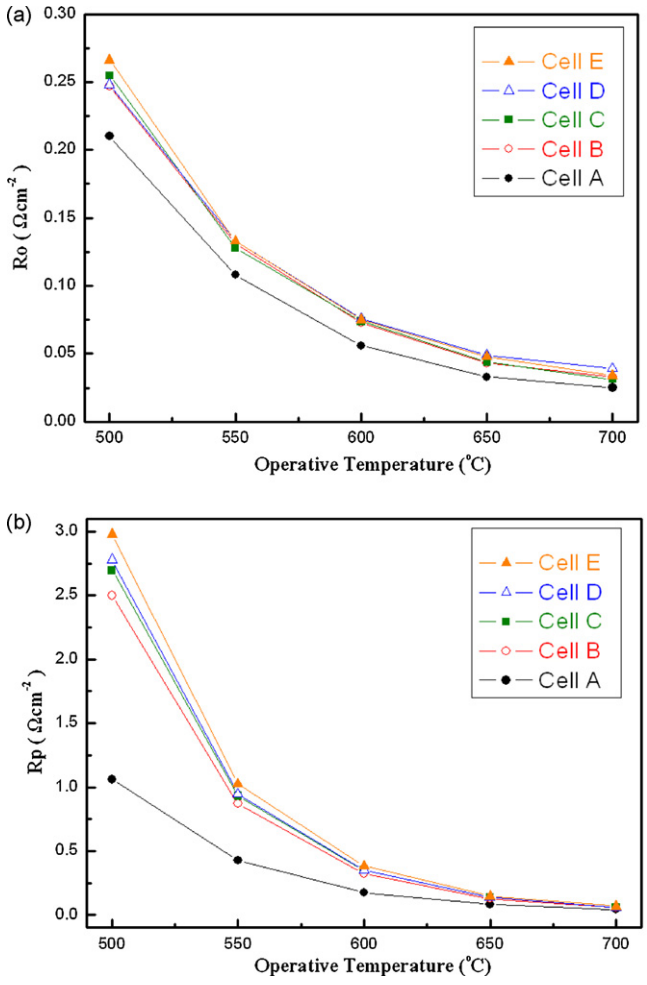

Fig. 7. Temperature dependences of (a) ohmic resistances (R_0) and (b) polarization resistances (R_P) for the anode-supported single cells containing bi-layer cathodes composed of a LSCF–SDC layer and a LSCF layer in various thicknesses (t_c represents the thickness of the LSCF–SDC composite cathode).

Polarization resistances of the single cells with various electrodes are shown in Table 2 and plotted in Fig. 7(b). It is evident that the R_P increased as the temperature decreased, particularly at temperatures ≤550 °C. As illustrated in Fig. 7(b), though the differences in R_P for all single cells were small at temperatures ranging from 550 to 700 °C, the R_P values of the single cells showed visible distinctions and followed the sequence of $R_{P,Cell\ E} > R_{P,Cell\ D} > R_{P,Cell\ C} > R_{P,Cell\ B} > R_{P,Cell\ A}$ within the temperature range of 600–700 °C. The polarization resistances of Cell B, Cell C, Cell D and Cell E demonstrated no significant difference and were all higher than that of Cell A with pure LSCF cathode. As the temperature was reduced to 500 °C, the difference in R_P values among the cells turned significant. The R_P value of the single cells at 500 °C seems to increase with the thickness of the LSCF–SDC composite layer in the cathode (1.02, 2.42, 2.62, 2.72, and 2.92 $\Omega\,cm^2$ for Cell A, Cell B, Cell C, Cell D, and Cell E, respectively). The R_P value of the Cell A (1.02 $\Omega\,cm^2$) at 500 °C was lower than most of the findings reported in the literature [15,16]. Comparing the polarization resistances of Cell A having a cathode of pure LSCF and Cell B, Cell C, Cell D, and Cell E having a bi-layer cathode, the study finds the addition of electrolyte SDC to LSCF unable to provide significant benefit to electrochemical performance of electrode. This is different from the situation observed in the YSZ–LSM and YSZ–SDC systems [24,25,29,32,33] in which the incorporation of YSZ or SDC into the LSM cathode layer significantly reduced the impedance of the cell due to the facts that introducing YSZ or SDC into the cathode resulted in a substantial increase in the ionic conductivity of the cathode and expanded the triple phase boundary region. Therefore, oxygen can be reduced to oxygen ions over a significant portion of the electrode surfaces, raising the number of sites available for the electrochemical activity. In this study, LSCF used as the cathode material reported a good single phase mixed ionic and electronic conductor. Though capable of improving the thermal expansion match and triggering a better adhesion to the electrolyte layer, addition of ionic conductor SDC into the LSCF does not enhance

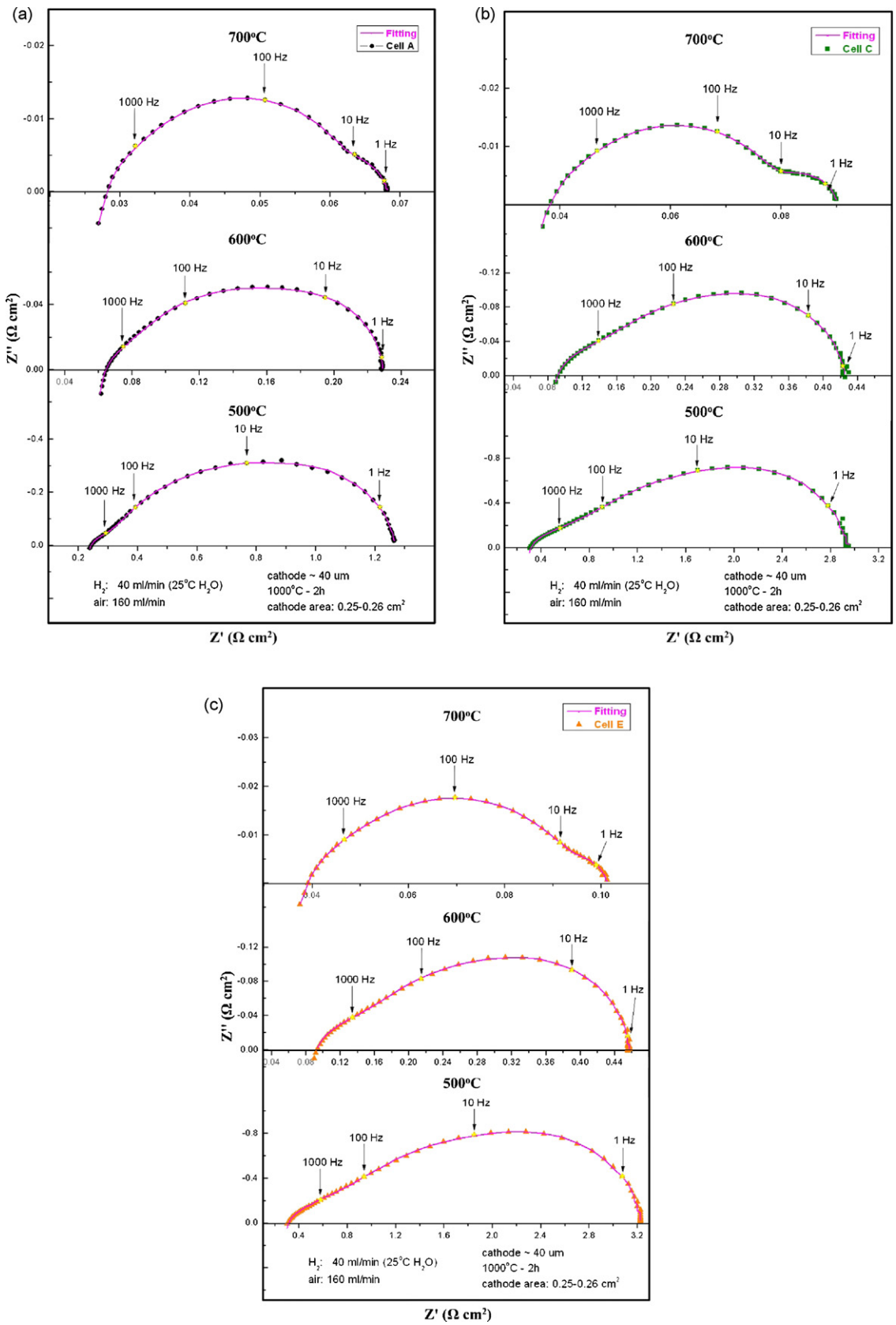

Fig. 8. Impedance spectra as a function of temperature for (a) Cell A, (b) Cell C, and (c) Cell E.

Table 3
Results of fitting electrochemical impedance spectra of anode-supported single cells measured at the temperatures ranging from 500 to 700 °C, under zero dc bias conditions.

	Impedance spectra fitting results for Cell A										
	Temperature (°C)	R_0 (Ω cm^2)	R_1 (Ω cm^2)	CPE_1-T (F cm^{-2})	CPE_1-P	R_2 (Ω cm^2)	CPE_2-T (F cm^{-2})	CPE_2-P	R_3 (Ω cm^2)	CPE_3-T (F cm^{-2})	CPE_3-P
Cell A	500	0.227	0.139	0.118	0.488	0.209	0.171	1.049	0.695	0.037	0.787
	550	0.121	0.093	0.197	1.082	0.095	0.055	1.037	0.228	0.104	0.625
	600	0.061	0.042	0.273	1.056	0.061	0.069	0.955	0.066	0.151	0.637
	650	0.036	0.018	0.455	0.992	0.042	0.093	0.874	0.021	0.167	0.665
	700	0.025	0.005	6.560	0.957	0.030	0.095	0.842	0.008	0.086	0.767
Cell B	500	0.276	0.276	0.005	0.647	0.732	0.039	1.004	1.478	0.024	0.647
	550	0.153	0.098	0.006	0.742	0.336	0.046	0.970	0.416	0.034	0.701
	600	0.081	0.049	0.027	0.984	0.164	0.054	0.932	0.102	0.052	0.595
	650	0.052	0.019	0.032	0.926	0.077	0.070	0.868	0.020	0.014	0.801
	700	0.037	0.004	9.476	1.005	0.039	0.096	0.774	0.008	0.015	0.890
Cell C	500	0.279	0.283	0.004	0.695	0.758	0.043	1.009	1.652	0.025	0.636
	550	0.125	0.129	0.007	0.716	0.377	0.044	0.944	0.430	0.030	0.704
	600	0.078	0.058	0.025	0.936	0.189	0.051	0.879	0.101	0.032	0.615
	650	0.043	0.031	0.261	0.595	0.083	0.093	0.781	0.024	0.105	0.565
	700	0.032	0.010	7.152	0.884	0.035	0.099	0.775	0.013	0.059	0.702
Cell D	500	0.277	0.296	0.005	0.646	0.802	0.041	0.988	1.672	0.024	0.631
	550	0.154	0.081	0.003	0.818	0.374	0.046	0.966	0.472	0.036	0.664
	600	0.085	0.052	0.022	1.030	0.170	0.057	0.941	0.119	0.048	0.594
	650	0.051	0.025	0.060	0.850	0.082	0.089	0.851	0.028	0.032	0.688
	700	0.038	0.004	12.592	0.999	0.046	0.122	0.751	0.011	0.031	0.776
Cell E	500	0.275	0.359	0.008	0.613	1.112	0.034	0.957	1.504	0.019	0.681
	550	0.152	0.144	0.008	0.703	0.497	0.039	0.933	0.369	0.023	0.770
	600	0.082	0.065	0.021	0.955	0.226	0.051	0.897	0.085	0.022	0.667
	650	0.048	0.032	0.069	0.774	0.098	0.091	0.824	0.019	0.016	0.761
	700	0.033	0.005	15.176	0.948	0.052	0.142	0.734	0.011	0.044	0.750

The CPE is defined by two values, CPE-T and CPE-P, and given by $1/T(j\omega)^P$.

superfluous in increasing the TPB in the cathode and may lead to a lower electrical conductivity of the cathode. It should be noted that the contribution of R_0 to the total resistance ($R_{tot} = R_0 + R_P$) is small due to the thinner electrode layer (13 μm). The ratio of R_P to R_{tot} read approximately 65% at 700 °C and increased dramatically as the operating temperature was reduced (>83% at 500 °C), implying that the performance of the cells depends critically on the polarization resistance. Successful development of catalytically active electrodes and interfaces is the key to render SOFCs more effective for operation at low temperatures (<600 °C).

In order to understand further the cathode polarization of the anode-supported SOFC cell, the impedance spectra as a function of temperature for Cell A, Cell C, and Cell E are shown in Fig. 8. They indicate three distinct time constants as evidenced by three semicircular features. The high-frequency semicircles in the Nyquist plots are mainly related to the charge transfer processes on the cathode while the low-frequency ones are primarily due to the mass transfer processes on the cathode [11]. The appearance of the semicircles reflects the rate-determining step in the processes of oxygen reduction on the cathode. It should be noted that the trends of the change in the impedance configuration with respect to temperature for various cells seem to be very similar, suggesting that the rate-limiting mechanisms at different temperatures among the cells are the same. The impedances corresponding to various frequencies, however, shift to a larger value as the thickness of the composite layer in the cell increases. For instance, at the temperature of 500 °C, the impedances measured at 1 Hz for Cell A, Cell C, and Cell E read, respectively, 2.22, 2.78, and 3.08 Ω cm^2.

The R_0 and R_P of the cells were extracted by fitting the experiment results of Fig. 6 to an equivalent circuit with configuration of $R_0(R_1 - CPE_1)_{HF}(R_2 - CPE_2)_{MF}(R_3 - CPE_3)_{LF}$ shown in Fig. 9. The simulation data are listed in Table 3. The impedance spectra are likely to be associated with the kinetic processes at the cathode since the contribution from the anode is small and can be ignored. The CPE is defined by two values, CPE-T and CPE-P, and given by $1/T(j\omega)^P$, where T and P are two parameters and ω the angular frequency. Examination of impedance spectra indicates that the size of the semicircle obtained in the high-frequency range ($R_1 - CPE_1$) is extremely small; contribution to R_{tot} can thus be ignored. It is further observed that the R_2 value is several times larger than the R_3 value at 700 °C. The medium-frequency semicircle is larger than the low-frequency semicircle in the Nyquist plots, suggesting that the processes associated with the low-frequency semicircle took place most rapidly on the cathode since the porosity of the cathode was high enough for oxygen diffusion as indicated by the SEM results (Fig. 4). The temperature exerts a disproportionate influence on the semicircles. The low-frequency (<10 Hz) semicircle became more capacitive than higher-frequency semicircles as the temperature dropped below 550 °C. The magnitude of increase in the R_3 value appeared to be more significant than that of the R_2 value as the temperature decreased. R_2 and R_3 were identified as the major contributors to electrode polarization, respectively, at temperatures above and below 550 °C.

Listed in Table 4, the activation energy values, E_0, E_1, E_2, and E_3 that corresponded, respectively, to the R_0, R_1, R_2, and R_3 values were obtained from linear regression in the Arrhenius plots of $1/R$. The E_1, E_2, and E_3 values of the Cell A are relatively lower as compared with those of other cells, yet the E_0 values remain similar among all cells. The addition of SDC-LSCF composite layer in the cathode appeared to raise the activation energy of the oxygen transfer process. The R_1, R_2, and R_3 values of the cells fell in the range of 0.004–0.359, 0.030–1.112, and 0.008–1.672 Ω cm^2, respectively, rising significantly with increase in the thickness of

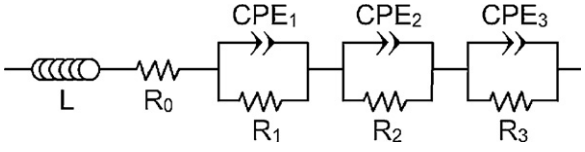

Fig. 9. The equivalent circuit used for the deconvolution of the fuel cell.

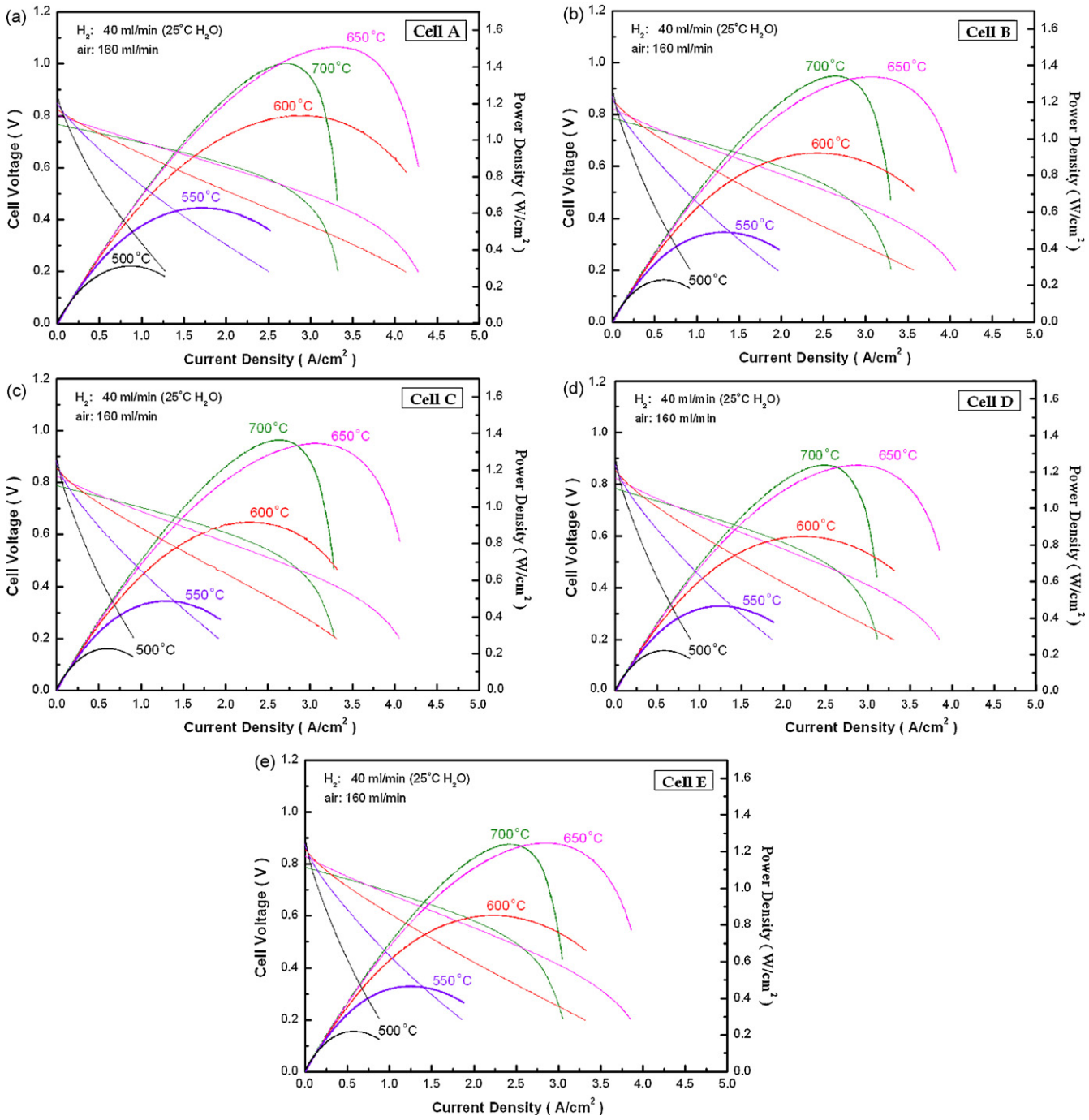

Fig. 10. *I–V* curves and the corresponding power densities of the anode-supported single cells containing bi-layer cathodes composed of a LSCF–SDC layer and a LSCF layer in various thicknesses. The thickness of the LSCF–SDC composite cathode (t_c): (a) 0 μm, (b) 10 μm, (c) 20 μm, (d) 30 μm, and (e) 40 μm, after electrochemical measurements.

Table 4
Activation energy values calculated for the R_1, R_2, and R_3 for various cells.

	Ea				
	E_0	E_1	E_2	E_3	Ep
Cell A	0.72	1.02	0.75	1.59	1.04
Cell B	0.66	1.29	0.94	1.74	1.26
Cell C	0.64	1.33	0.98	1.63	1.23
Cell D	0.66	1.25	0.93	1.66	1.24
Cell E	0.70	1.26	1.02	1.58	1.22

Ea: activation energy, eV.

the SDC-LSCF in the bi-layer cathode or decrease in the operation temperature. For the high-frequency semicircle, the corresponding activation energies for $1/R_1$ of various cells ranged from 1.03 to 1.33 eV. The present results are similar to those reported in the literature [25,34,35]. A similar interpretation can therefore be made that the first semicircle at high frequency corresponds to the transport of oxygen ions at the electrode–electrolyte interface. For the second one at medium frequency, the activation energies of $1/R_2$ stretched over a range of 0.75–1.02 eV, appearing to be associated with the atomic oxygen diffusion within the electrode followed by a charge transfer [35–37] and indicating thereby that atomic oxygen diffusion and charge transfer may be the rate-limiting mechanisms at temperatures above 550 °C. Finally, for the third semicircle at

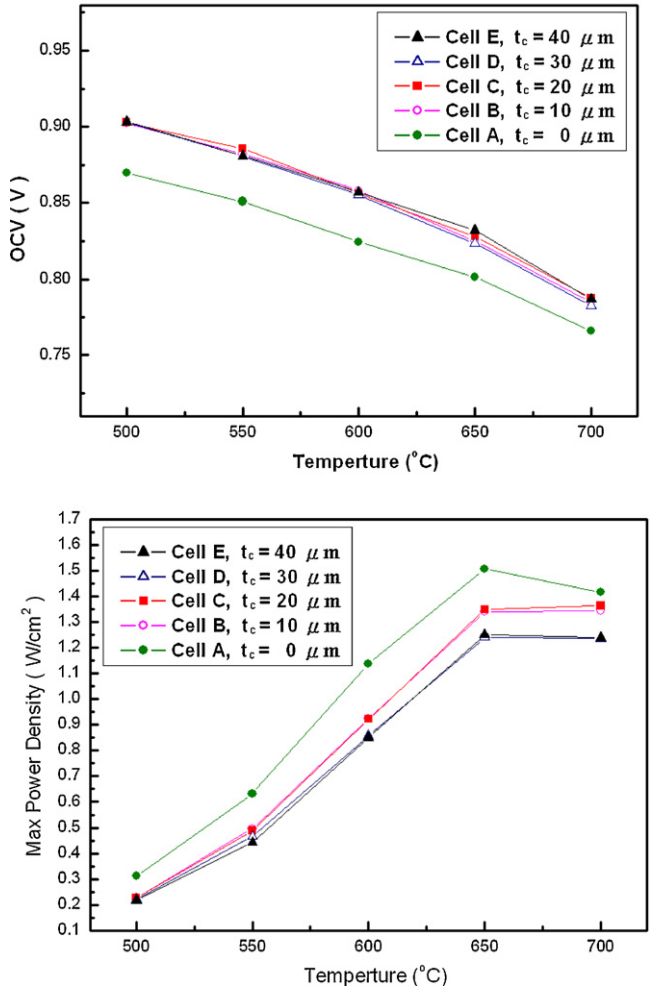

Fig. 11. Temperature dependences of OCV and maximum power density for the anode-supported single cells containing bi-layer cathodes composed of a LSCF–SDC layer and a LSCF layer in various thicknesses (t_c represents the thickness of the LSCF–SDC composite cathode).

low frequency, the activation energies of $1/R_3$ were in the ranges of 1.58–1.74 eV, a result similar to those reported by Murray et al. for the LSM–GDC and LSM–YSZ systems [24]. It can thus be concluded that molecular oxygen adsorption and dissociation phenomena are a rate-determining step at temperature below 550 °C. This process is characterized by relative high values of CPE-P and E values [25,36,38].

The cell performance as a function of operating temperature for single cells with various cathodes is shown in Fig. 10. The open circuit voltage (OCV) of the single cells decreased with the rise in temperature, dropping from 0.87–0.90 V at 500 °C to 0.77–0.79 V at 700 °C. These OCV values are lower than the expected theoretical values at higher temperatures, which is due to the mixed ionic and electronic conduction of the SDC electrolyte in the reducing atmosphere [5]. Part of the Ce^{4+} ions in the electrolyte were reduced to Ce^{3+} ions, causing some electronic conduction in the electrolyte and resulting in OCV drop. With decreasing temperature, OCV gradually moved up as the electronic conduction went down at lower temperatures. As indicated in Fig. 11(a), Cell A has the lowest OCV (0.87 V) and Cell E the highest (0.90 V) at 500 °C. Taking into consideration of the thickness of the single cell as a whole, it is apparent that the thicker the SDC-containing layer (SDC electrolyte layer and LSCF–SDC composite active layer), the lesser the electronic conduction and the higher the OCV. Moreover, as observed in the NiO–YSZ–LSM SOFC system reported by Reitz et al. [32,39], insertion of interlayer NiO–YSZ and LSM–YSZ at the anode/electrolyte and electrolyte/cathode interfaces increases the OCV of the cell, due to the better thermal expansion matching and the subsequent greater integrity of the cell. Maximum power densities (MPD) of the single cells operated at various temperatures are plotted in Fig. 11(b). MPD declined with decreasing operating temperature due to the increase of the R_0 and R_P of the single cells shown in Fig. 7. Cell A was observed to report the highest MPD and Cells D and E the lowest at all temperatures measured among the single cells. Maximum MPDs for all single cells (1.5, 1.3, 1.3, 1.2, and 1.2 W cm^{-2} for Cell A, Cell B, Cell C, Cell D, and Cell E, respectively) were obtained at 650 °C. The MPDs at 700 °C were equivalent to or lower than those at 650 °C for most cells since the electrolyte layer of SDC possessed a higher electronic conduction that led to a lower OCV at 700 °C, and the cells reported a higher degree of concentration polarization at 700 °C as indicated by the convex-up curvature of the I–V curves at high current densities as shown in Fig. 10. Cells B, Cell C, Cell D and Cell E appeared to have similar MPDs at the various temperatures measured. According to the results, Cell A with a cathode of pure LSCF is marked by the lowest impedance, the lowest OCV, and the highest MPD. A single cell with a bi-layer cathode composed of a LSCF–SDC composite layer and a LSCF layer tends to increase the impedance and OCV and decrease the MPD with growth in the thickness of the composite layer. This is different from those observed in the YSZ–LSM system in which the insertion of the composite layer in the cathode reduces the impedance and thus increases the MPD of the cell. Considering both the electrical and the mechanical integrity of the single cell, insertion of the composite layer is required to guarantee a good adhesion of the cathode layer to the electrolyte layer. However, the thickness of the composite layer should be kept as thin as possible so as to minimize the R_0 and R_P and maximize the cell performance.

4. Conclusions

In this study, anode-supported planar IT-SOFCs, with a thin SDC electrolyte film and a bi-layer cathode composed of a current collector LSCF layer and a functional LSCF–SDC composite layer in various thicknesses, were fabricated using tape-casting and screen-printing processes. Major conclusions reached by the study are summarized as follows:

1. The obtained SDC electrolyte with a thickness of approximately 13 μm appeared to be crack free and dense with several scattering closed pores. The interfaces among the anode, electrolyte, and cathode layers for all cells showed good adhesion, except for Cell A that could be detached easily from the surface of the electrolyte film after the electrochemical test, due to thermal expansion mismatch.
2. At operation temperature of 500 °C, the R_P of Cell A (1.247 Ω cm^2) emerged to be the lowest in the single cells while the R_P value was observed to increase with the thickness of the LSCF–SDC layer in the cathode. This indicates that the high electrical conductivity of the cathode serves as a major contributing factor for reducing the R_P at 500 °C.
3. The open circuit voltage of the single cells decreased with the rise in temperature, dropping from 0.87–0.90 V at 500 °C to 0.77–0.79 V at 700 °C. Maximum MPDs for all single cells were obtained at 650 °C. Cell A with a cathode of pure LSCF layer showed a maximum power density of 1.51 W cm^{-2} and an open circuit voltage of 0.80 V, however, the long term reliability was compromised due to mechanical and thermal mismatch with the electrolyte material.

4. Though the addition of SDC to LSCF can improve the adhesion of the cathode layer to electrolyte layer, the thickness of the composite layer should be as thin as possible to minimize the R_0 and R_P and maximize the cell performance.

References

[1] M.D. Mat, X. Liu, Z. Zhu, B. Zhu, Int. J. Hydrogen Energy 32 (2007) 796–801.
[2] T.L. Wen, D. Wang, M. Chen, H. Tu, Z. Zhang, H. Nie, W. Huang, Solid State Ionics 148 (2002) 513–519.
[3] E. Ivers-Tiffée, A. Weber, D. Herbstritt, J. Eur. Ceram. Soc. 21 (2001) 1805–1811.
[4] M. Zhang, M. Yang, Z. Hou, Y. Dong, M. Cheng, Electrochim. Acta 53 (2008) 4998–5006.
[5] J.W. Fergus, J. Power Sources 162 (2006) 30–40.
[6] S.B. Adler, Chem. Rev. 104 (2004) 4791–4843.
[7] J.M. Ralph, A.C. Schoeler, M. Krumpelt, J. Mater. Sci. 36 (2001) 1161–1172.
[8] J.M. Ralph, C. Rossignol, R. Kumar, J. Electrochem. Soc. 150 (2003) A1518–A1522.
[9] W. Guo, J. Liu, C. Jin, H. Gao, Y. Zhang, J. Alloys Compd. 473 (2009) 43–47.
[10] P. Ried, P. Holtappels, A. Wichser, A. Ulrich, T. Graule, J. Electrochem. Soc. 155 (2008) B1029–B1035.
[11] H.C. Yu, F. Zhao, A.V. Virkar, K.Z. Fung, J. Power Sources 152 (2005) 22–26.
[12] M. Liu, D. Dong, F. Zhao, J. Gao, D. Ding, X. liu, G. Meng, J. Power Sources 182 (2008) 585–588.
[13] J. Piao, K. Sun, N. Zhang, S. Xu, J. Power Sources 175 (2008) 288–295.
[14] Y. Guo, H. Shi, R. Ran, Z. Shao, Int. J. Hydrogen Energy 34 (2009) 9496–9504.
[15] Y. Leng, S.H. Chan, Q. Liu, Int. J. Hydrogen Energy 33 (2008) 3808–3817.
[16] J. Zhang, Y. Ji, H. Gao, T. He, J. Liu, J. Alloys Compd. 395 (2005) 322–325.
[17] J. Chen, F. Liang, B. Chi, J. Pu, S.P. Jiang, L. Jian, J. Power Sources 194 (2009) 275–280.
[18] F. Liang, J. Chen, S.P. Jiang, B. Chi, J. Pu, L. Jian, Electrochem. Solid State Lett. 11 (2008) B213–B216.
[19] X. Ding, X. Kong, J. Jiang, C. Cui, L. Guo, Int. J. Hydrogen Energy 35 (2010) 1742–1748.
[20] R.N. Basu, A.D. Sharma, A. Dutta, J. Mukhopadhyay, Int. J. Hydrogen Energy 33 (2008) 5748–5754.
[21] C. Jin, J. Liu, W. Guo, Y. Zhang, J. Power Sources 183 (2009) 506–511.
[22] X. Ding, C. Cui, L. Guo, J. Alloys Compd. 481 (2008) 845–850.
[23] J. Van Herle, R. Ihringer, R. Vasquez Cavieres, L. Constantin, O. Bucheli, J. Eur. Ceram. Soc. 21 (2001) 1855–1859.
[24] E.P. Murray, T. Tsai, S.A. Barnett, Solid State Ionics 110 (1998) 235–243.
[25] E.P. Murray, S.A. Barnett, Solid State Ionics 143 (2001) 265–273.
[26] Fuel Cell Handbook, 7th edition, EG&G Technical Services, Inc., USDOE (2004), pp. 7–18.
[27] Q.A. Huang, R. Hui, B. Wang, J. Zhang, Electrochim. Acta 52 (2007) 8144–8164.
[28] C. Xia, M. Liu, Adv. Mater. 14 (2002) 521–523.
[29] C. Fu, S.H. Chan, Q. Liu, X. Ge, G. Pasciak, Int. J. Hydrogen Energy 35 (2010) 301–307.
[30] X. Xu, C. Xia, G. Xiao, D. Peng, Solid State Ionics 176 (2005) 1513–1520.
[31] H.J. Hwang, J.W. Moon, S. Lee, E.A. Lee, J. Power Sources 145 (2005) 243–248.
[32] T.L. Reitz, H. Xiao, J. Power Sources 161 (2006) 437–443.
[33] X. Xu, Z. Jiang, X. Fan, C. Xia, Solid State Ionics 177 (2006) 2113–2117.
[34] M.J. Escudero, A. Aguadero, J.A. Alonso, L. Daza, J. Electroanal. Chem. 611 (2007) 107–116.
[35] M. Prestat, A. Infortuna, S. Korradi, S. Rey-Mermet, P. Muralt, L.J. Gauckler, J. Electroceram. 18 (2007) 111–120.
[36] R. Barfod, A. Hagen, S. Ramousse, P.V. Hendriksen, M. Mogensen, Fuel Cells 06 (2006) 141–145.
[37] R. Barfod, M. Mogensen, T. Klemenso, A. Hagen, Y.L. Liu, P.V. Hendriksen, J. Electrochem. Soc. 154 (2007) B371–B378.
[38] S.P. Yoon, J. Han, S.W. Nam, T.H. Lim, I.H. Oh, S.A. Hong, Y.S. Yoo, H.C. Lim, J. Power Sources 106 (2002) 160–166.
[39] K. Chen, X. Chen, Z. Lu, N. Ai, X. Huang, W. Su, Electrochim. Acta 53 (2008) 7825–7830.